Reversibility Of Superconducting Nb Weak Links Driven By The Proximity Effect In A Quantum Interference Device

Nikhil Kumar,[1] T. Fournier,[2,3] H. Courtois,[2,3] C. B. Winkelmann,[2,3] and Anjan K. Gupta[1,*]

[1]*Department of Physics, Indian Institute of Technology Kanpur, Kanpur 208016, India*
[2]*Université Grenoble Alpes, Institut Néel, F-38042 Grenoble, France*
[3]*CNRS, Institut Néel, F-38042 Grenoble, France*

We demonstrate the role of the proximity effect in the thermal hysteresis of superconducting constrictions. From the analysis of successive thermal instabilities in the transport characteristics of micron-size superconducting quantum interference devices with a well-controlled geometry, we obtain a complete picture of the different thermal regimes. These determine whether or not the junctions are hysteretic. Below the superconductor critical temperature, the critical current switches from a classical weak-link behavior to one driven by the proximity effect. The associated small amplitude of the critical current makes it robust with respect to the heat generation by phase slips, leading to a nonhysteretic behavior.

Micron-size superconducting quantum interference devices (μ-SQUID), based on superconducting (SC) weak links (WLs), have been of interest for probing magnetism at small scales [1–8]. A major obstacle of a μ-SQUID proper operation is its hysteretic current-voltage characteristic (IVC). During current ramp-up, the WL switches to a dissipative state at the critical current I_c, and during current ramp-down, it comes back to a zero-voltage state at the retrapping current $I_r < I_c$. In conventional tunnel-barrier-type Josephson junctions, the hysteresis arises from large junction capacitance [9]. In WLs with negligible capacitance, hysteresis is found at low temperatures below a crossover temperature $T_h < T_c$ [10], with T_c as the SC critical temperature. Although an effective capacitance can arise from the recovery time of the SC order parameter [11], it is now understood that hysteresis in WLs is of thermal origin [12–14], similar to that observed in SNS WLs [15]. A recent report on high-T_c-SC based μ-SQUID shows nonhysteretic IVCs over a wide temperature range [16]. Thermal hysteresis in WLs and its effect on IVCs has been modeled by local thermal balance dictating the position of a normal metal-superconductor (N-S) interface [12–14]. In the case of poor heat evacuation, phase fluctuations can trigger a thermal runaway giving a resistive hot spot. This topic is of great practical importance, in particular, for SC-magnet wires and cables, helium level sensors, bolometers [17], μ-SQUIDs, and other nanoscale SC structures [18]. A systematic understanding of various thermal phases which a WL device exhibits can help in designing nonhysteretic devices.

In this Letter, we report on the transport characteristics of Nb-film based μ-SQUIDs with a well-controlled geometry and describe a complete picture of different thermal regimes. The IVCs show a critical current and two retrapping currents that we describe using a thermal instability model in SC leads. The critical current I_c follows the theoretical expectation at low temperatures but changes its behavior while crossing the smaller retrapping current. In this hysteresis-free regime, the WLs super-conduct, despite being slightly heated by individual phase slips, thanks to the proximity effect of the adjacent SC.

We fabricated [19] μ-SQUIDs from Nb films using common techniques [2,20,21]. The transport measurements were carried out down to 4.2 K in a homemade cryostat with built-in copper-powder filters [10]. We have studied six devices with similar behavior, but here we report on two devices, $\mu S1$ and $\mu S2$. For all devices, the patterned SQUID-loop area is 1 μm^2 and the width of its arms is 0.3 μm. The designed WL length is 150 nm, while the WL width is 70 and 50 nm in $\mu S1$ and $\mu S2$, respectively. Figure 1(a) shows the SEM image of $\mu S1$. Four different parts of the pattern contribute to the electrical characteristics, namely, (1) the two WLs, each of normal resistance R_{WL}, (2) the SQUID loop with normal resistance as R_L, including the WLs, (3) the narrow leads of width 0.3 μm and length 1.7 μm on either side of the SQUID loop, each with a resistance R_1, and (4) the wide leads of width 2 μm, length 27.5 μm, and normal resistance R_2. From the geometry, the total normal-state resistance between the voltage leads is $R_N = R_L + 2R_1 + 2R_2 = 40.3R_\square + 0.5R_{\mathrm{WL}}$. Here, $R_\square$ is the film's square resistance.

Figures 1(b) and 1(c) show the resistance R versus temperature for $\mu S1$. Multiple SC transitions are observed. The resistance jumps from its residual value of 128 Ω down to about 40 Ω at $T_{c2} = 8.7$ K, jumps further down from 38 to 8 Ω at $T_{c1} = 8.35$ K, and finally decreases smoothly to zero. We attribute the transition at T_{c2} to the wide leads and that at T_{c1} to both the narrow leads and the SQUID loop.
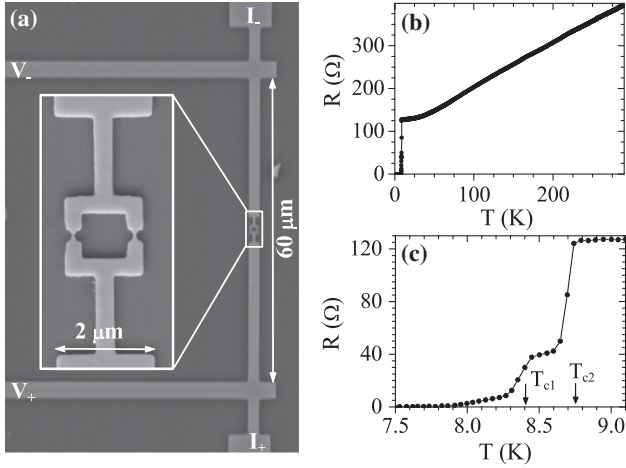
FIG. 1. (a) SEM image of the μ-SQUID $\mu S1$ with its current and voltage leads. The zoomed-in image shows the SQUID loop (with area $1 \times 1 \ \mu m^2$) and the narrow leads. (b) Resistance versus temperature (R-T) plot. (c) Low-temperature portion of the R-T plot for $\mu S1$ at 0.01 mA current.

FIG. 2 (color online).   (a) Schematic of the semi-infinite (in $+x$ direction) lead of SC material on a substrate at T_b with an N-S interface at $x = 0$. Panel (b) shows the region near the N-S interface with three differential elements of length dx when the N-S interface stabilizes near the heat source on the left.

From IVC in the nonhysteretic regime, discussed later [see Fig. 3(f)], we deduce $R_{WL} \simeq 8 \ \Omega$. This analysis is consistent with $R_{\square} = 3.1 \ \Omega$, giving a resistivity of $9.5 \ \mu\Omega \cdot$ cm.

Next we discuss a one-dimensional model of thermal instability in long current-biased SC leads. This is similar to the Broom and Rhoderick [22] model on the dynamics of an N-S interface under the influence of a current. Thus, a critical magnitude of the current is found at which the N-S interface changes its direction of motion. Here we consider a SC lead with normal state resistivity ρ_n, uniform thickness t and width w, and carrying an electrical current I as shown in Fig. 2(a). The heat transfer with the substrate at a bath temperature T_b is written $\alpha(T - T_b)/t$, where α is a characteristic of the interface. The thermal conductivity κ is constant and uniform. An N-S interface exists at $x = 0$, so at this point $T = T_c$. A heat current flows from $x < 0$ due to the resistance of this lead portion plus possibly a device at the end of the lead. With the boundary condition $T = T_b$ at $x \rightarrow \infty$, the heat equation solution for $x > 0$ is $T = T_b + (T_c - T_b) \exp(-x/l_{th})$. The thermal healing length $l_{th}(= \sqrt{\kappa t/\alpha})$ is a crossover length scale such that for $\Delta x \gg l_{th}$ substrate heat loss dominates and for $\Delta x \ll l_{th}$ conduction dominates. The heat current at the N-S interface ($x = 0$) is then $\dot{Q}_0 = w\alpha l_{th}(T_c - T_b)$, implying an effective thermal resistance of $(w\alpha l_{th})^{-1}$ as seen from the N-S interface. It is important to realize that the N-S interface will shift to the right (left) if more (less) than $\dot{Q}_0$ heat is incident on the lead at $x = 0$.

For analyzing the stability of the N-S interface, we look into the effect of fluctuations on a differential element (from $x = 0$ to $x = dx$) at this interface in a quasistatic approximation. If this element 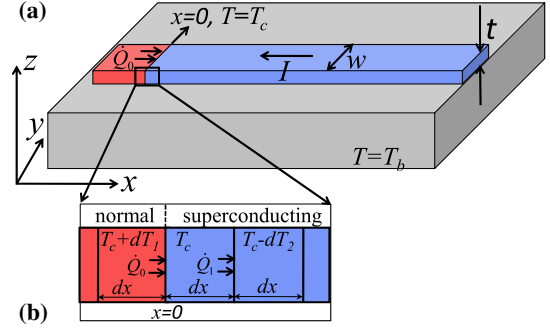becomes resistive [see Fig. 2(b)], an additional power $I^2 \rho_n dx/(wt)$ is generated, which is shared equally between the left and right interfaces to the lead, and the substrate receives a negligible amount [19]. The heat current across the new N-S interface is $\dot{Q}'_1 = \dot{Q}_0 - \alpha(T_c - T_b)wdx + I^2\rho_n dx/(2wt)$. As pointed out before, if this heat is more (less) than $\dot{Q}_0$, the N-S interface will shift to the right (left), implying instability (stability). Thus, the maximum current that the lead can carry without causing a thermal instability is given by

$$I_{max} = w\sqrt{2\alpha(T_c - T_b)/R_{\square}}. \qquad (1)$$

This expression is consistent with the results of Ref. [12] in the long lead limit and equal thermal conductivities of SC and normal metal, which is valid close to the N-S interface. When I exceeds I_{max}, the N-S interface will run away to a large x location where the lead joins a thermal bath (or a much wider lead). By analyzing the stability of a small resistive element against an incursion to the SC state, one finds, as expected, the same expression for the retrapping current. It would be more appropriate to call I_{max} the "instability current" as it describes both the runaway and the retrapping of the N-S interface. We will use the term "retrapping" current, as has been done in most of the earlier works.

In order to quantify the relevant parameters, we use the Wiedemann-Franz law, i.e., $\kappa = LT/\rho$ with $L = 2.44 \times 10^{-8} \ W\Omega/K^2$ as the Lorenz number; using $T = T_c = 8.5$ K and $\rho = 9.5 \ \mu\Omega$ cm, we get $\kappa = 2.4 \ W/m$ K. Typical values of α used in the literature [12,14] range from 1 to 10 W/cm^2 K. We use $\alpha = 5.3 \ W/cm^2$ K, which is found from the temperature dependence of a retrapping current as discussed later. Thus, we find $l_{th} = 1.6 \ \mu$m for our devices, which is much smaller than the length of the wide leads and comparable to that of the narrow leads.

IVCs of $\mu S1$ in Fig. 3 show sharp jumps in voltage at three currents, namely, I_{r1}, I_{r2}, and I_c. The jump at I_c occurs during the current ramp up from zero with a
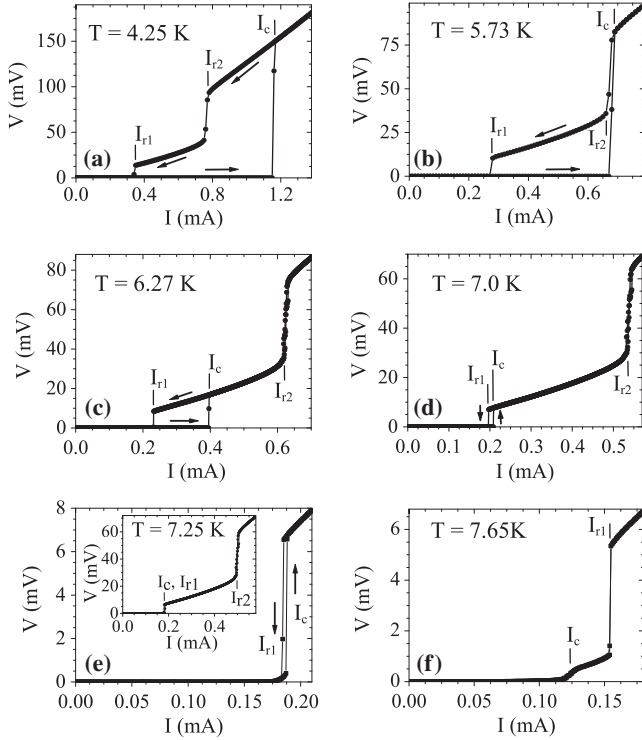
FIG. 3.   (a)-(d) IVCs in the hysteretic regime for $\mu S1$ at different temperatures. A large hysteresis is seen at 4.25 K with two retrapping currents, I_{r1} and I_{r2}. I_c crosses I_{r2} near 5.7 K and I_{r1} around 7.25 K as seen in (e). Panel (f) shows the IVC of $\mu S1$ in the nonhysteretic regime above $T_h = 7.25$ K. The inset of (e) gives a larger bias-current range plot to show the I_{r2} transition.

distribution in its value. Thus, for $\mu S1$ I_c has a width [19] of about 40 μA with a mean value of 1.3 mA at 4.2 K, in agreement with the expected depairing current [23]. From the IVC slope, the resistance just above I_{r1} is about 48 Ω. This value is close to the sum $R_L + 2R_1 = 40\ \Omega$, which means that the SQUID loop and the narrow leads are heated to above T_c for $I > I_{r1}$. The observed higher value indicates that a portion of the wide leads is also heated to above its T_c. The IVC slope above the second retrapping current I_{r2} is 140 Ω, which is close to the measured residual resistance value, i.e., 128 Ω, indicating a thermal runaway until the voltage leads. The slightly larger value seen here is due to the heating in the central portion to more than 50 K as estimated from a thermal model. At higher temperatures when I_{r2} is much lower, indicating reduced heating, the slope above I_{r2} is found to be 128 Ω. In this regime, Fig. 3(f) shows that the resistance just above I_c is about 4 Ω, giving $R_{WL} = 8\ \Omega$. Only I_c was found to oscillate with the magnetic flux [19], as expected for a SQUID. The retrapping currents $I_{r1,2}$ do not oscillate, implying a different origin than the SC of the WL.

The three currents I_{r1}, I_{r2}, and I_c evolve differently with temperature. Near 5.7 K, I_c crosses I_{r2} [see Fig. 3(b)] and at $T = T_h = 7.25$ K, I_c crosses I_{r1} [see Fig. 3(e)], so the hysteresis is absent at higher temperatures [see Fig. 3(f)]. In

the nonhysteretic regime above T_h, the IVC near I_c becomes relatively smooth while the voltage jump at I_{r1} remains sharp and evolves over this smooth feature. Also, the hysteresis does not disappear until I_{r1} fully crosses this smooth feature [see Fig. 3(e)].

Figure 4(a) summarizes the T_b dependence of I_c, I_{r1}, and I_{r2} for $\mu S1$. Figure 4(b) shows the same for the device $\mu S2$, with a smaller I_c, and thus a smaller T_h. The retrapping currents $I_{r1,2}$ are the same in the two samples, confirming that these are independent of the WL structure. With increasing T_b, I_c decreases linearly in both devices up to T_h, where it shows a marked change in behavior. For both devices, I_c and I_{r1} go to zero at T_{c1}, while I_{r2} vanishes at T_{c2}. This is consistent with the R-T behavior in Fig. 1(c). In both plots, we also indicate the state (resistive or SC) of different portions of the device when the current is ramped down, which constitutes a kind of phase diagram or, more
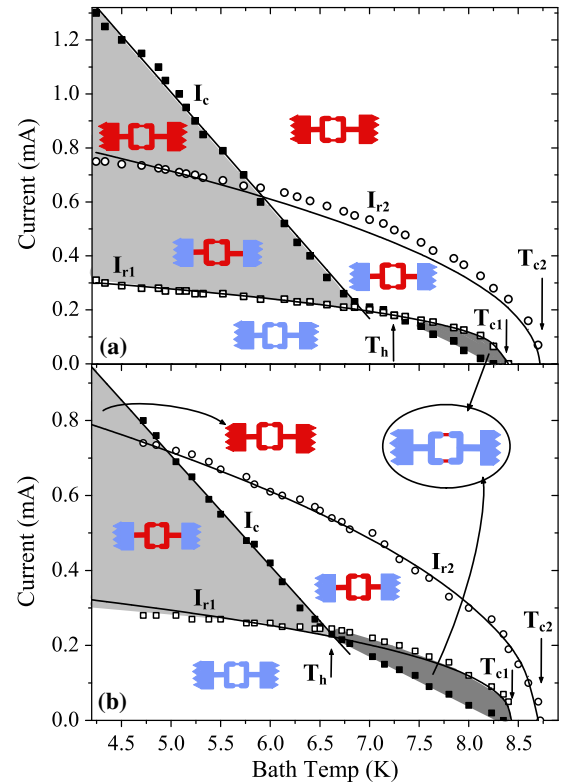

FIG. 4 (color online).   Variation of I_c, I_{r1}, and I_{r2} with T_b for (a) $\mu S1$ and (b) $\mu S2$. The symbols are the data points. The continuous lines are fits given by (in mA and K) (a) $I_c = 0.42(7.4 - T_b)$ and (b) $I_c = 0.29(7.4 - T_b)$, while the other two are described by $I_{r1} = 0.17(8.4 - T_b)^{0.43}$ and $I_{r2} = 0.37(8.7 - T_b)^{0.5}$ for both of the devices. The cartoon pictures of the device shown in different regions depict the state of the device during current ramp-down, with blue showing SC and red showing the resistive portions. The light gray-shaded area shows the bistable region where the whole device is in the fully SC state during the current ramp-up from zero. In the dark gray-shaded region, only WLs are resistive.

appropriately, state diagram. The light gray-shaded area shows the bistable region where the whole device is SC during the current ramp-up from zero. In the dark gray-shaded region, only the WLs are resistive. No hysteresis is observed in the related temperature range $[T_h, T_{c1}]$. This is the most desirable mode for a SQUID, but it occurs in quite a limited temperature window. At a fixed current bias, we do see the expected voltage oscillations with flux in this regime [19].

Using the long lead approximation for the wide leads, we can fit I_{r2} with Eq. (1), which is written here as $I_{r2} = w\sqrt{2\alpha(T_{c2} - T_b)/R_\square}$. We obtain a very good fit (see Fig. 4), with the only free parameter being $\alpha = 5.3$ W/cm^2 K, in good agreement with reported values [12,14]. With the same parameters, except $w = 0.3$ μm, Eq. (1) predicts, for the narrow leads, a current I_{r1} significantly smaller than observed. This is expected as the presence of wide leads at a short distance makes the heat evacuation more efficient, leading to a higher runaway current.

In a WL with dimensions less than the SC coherence length, we expect, close to its T_c, $I_c R_{WL} = \beta(T_c - T_b)$ with $\beta = 0.635$ mV/K [3]. Our devices are in the Josephson regime [3], at least close to T_c. From the I_c slope in Fig. 4(a) for $\mu S1$ at temperatures below T_h, we find an $R_{WL}/2$ value of 3 Ω, which agrees with our earlier findings. In this same regime, the extrapolated T_c value of 7.4 K is related to the intrinsic SC of the WLs. Above T_h, the T_b dependence of I_c changes slope and I_c goes to zero precisely at T_{c1}. Hence, we conclude that the WLs are SC above T_h owing to the proximity effect from the adjacent SC with a higher T_c.

Finally, we elaborate on how the behavior change of I_c coincides with T_h. Below T_h, I_c exceeds the stability current I_{r1}. In this case, even a single phase-slip event induced by thermal fluctuations can cause a thermal runaway [18]. IVCs thus exhibit a sharp voltage jump at I_c with a distribution in I_c values [24] because the transition is caused by stochastic fluctuations. Above T_h, $I_c < I_{r1}$, so that no thermal runaway can happen at I_c: The reversible (monostable) regime is obtained. The transition to the resistive state (at I_c) is smeared with a finite voltage below I_c [see Fig. 3(e)]. This is due to phase-slip proliferation as the energy barrier for the phase slip is small for currents close to I_c [24]. The related dissipation just below I_c also heats some portion of the device above T_b. Assuming that the whole SQUID loop is at nearly uniform temperature, which is justified since its size is comparable to l_{th}, we estimate that the power generated just below I_c of 72 nW for $T_b = 7.25$ K brings the SQUID loop to a temperature of about 7.8 K. Because of this and of the fact that the WL region is actually a SC with a lower T_c, the T_b dependence of I_c between T_h and T_{c1} cannot be simply described by that of S-N-S WLs [25]. Nevertheless, close to T_c we can expect a linear temperature dependence, as is the case with both SNS WL and constriction [3]. The heating will reduce

the I_c value, and the exact temperature dependence, close to T_c, would be sublinear.

I_c and I_{r1} are expected to cross at some temperature even if the WL T_c is the same as that of the adjacent SC. But then the reversible regime will exist over a narrower temperature range. Thus, the smaller T_c of the WL and the proximity SC play a crucial role in widening this hysteresis-free temperature range. By reducing the width of the constriction while keeping other dimensions the same, one can reduce I_c without affecting I_{r1}. This will definitely widen the temperature range of the reversible operation. Although at extremely low temperatures, due to divergent Kapitza resistance making α approach zero, the hysteresis is expected to occur even for very small I_c. This regime is yet to be investigated.

In conclusion, we present the complete device-state diagram of Nb based μ-SQUIDS. We highlight a nonclassical weak-link behavior which is understood in the framework of a thermal instability picture. The nonhysteretic high temperature regime of the weak links is shown to benefit from proximity superconductivity. The present new understanding of the physical mechanisms at the origin of a nonhysteretic behavior is key to further developments in μ-SQUID magnetosensors for which the suppression of hysteresis represents a key issue.

*Corresponding author.
anjankg@iitk.ac.in

[1] W. Wernsdorfer, Adv. Chem. Phys. **118**, 99 (2009).

[2] K. Hasselbach, C. Veauvy, and D. Mailly, Physica (Amsterdam) **332C**, 140 (2000).

[3] K. K. Likharev, Rev. Mod. Phys. **51**, 101 (1979).

[4] D. Hazra, J. R. Kirtley, and K. Hasselbach, Appl. Phys. Lett. **103**, 093109 (2013).

[5] D. Vasyukov et al., Nat. Nanotechnol. **8**, 639 (2013).

[6] A. G. P. Troeman, H. Derking, B. Borger, J. Pleikies, D. Veldhuis, and H. Hilgenkamp, Nano Lett. **7**, 2152 (2007).

[7] L. Hao, J. C. Macfarlane, J. C. Gallop, D. Cox, J. Beyer, D. Drung, and T. Schurig, Appl. Phys. Lett. **92**, 192507 (2008).

[8] Nicholas C. Koshnick, Martin E. Huber, Julie A. Bert, Clifford W. Hicks, Jeff Large, Hal Edwards, and Kathryn A. Moler, Appl. Phys. Lett. **93**, 243101 (2008).

[9] M. Tinkham, Introduction to Superconductivity, 2nd ed. (McGraw-Hill, New York, 1996).

[10] D. Hazra, Hysteresis in superconducting weak links and micron size superconducting interference devices, Ph.D thesis, IIT Kanpur (2011).

P H Y S I C A L R E V I E W L E T T E R S

[11] Y. Song, J. Appl. Phys. **47,** 2651 (1976); S. Michotte, S. Mátéfi-Tempfli, L. Piraux, D. Y. Vodolazov, and F. M. Peeters, Phys. Rev. B **69,** 094512 (2004).

[12] W. J. Skocpol, M. R. Beasley, and M. Tinkham, J. Appl. Phys. **45,** 4054 (1974).

[13] M. Tinkham, J. U. Free, C. N. Lau, and N. Markovic, Phys. Rev. B **68,** 134515 (2003).

[14] D. Hazra, L. M. A. Pascal, H. Courtois, and A. K. Gupta, Phys. Rev. B **82,** 184530 (2010).

[15] H. Courtois, M. Meschke, J. T. Peltonen, and J. P. Pekola, Phys. Rev. Lett. **101,** 067002 (2008).

[16] R. Arpaia, M. Arzeo, S. Nawaz, S. Charpentier, F. Lombardi, and T. Bauch, Appl. Phys. Lett. **104,** 072603 (2014).

[17] K. S. Ilin, M. Lindgren, M. Currie, A. D. Semenov, G. N. Goltsman, R. Sobolewski, S. I. Cherednichenko, and E. M. Gershenzon, Appl. Phys. Lett. **76,** 2752 (2000).

[18] N. Shah, D. Pekker, and P. M. Goldbart, Phys. Rev. Lett. **101,** 207001 (2008).

[19] See Supplemental Material at http://link.aps.org/supplemental/10.1103/PhysRevLett.114.157003 for fabrication details, SQUID oscillations and heat sharing during resistive fluctuation.

[20] L. Angers, F. Chiodi, G. Montambaux, M. Ferrier, S. Guéron, H. Bouchiat, and J. C. Cuevas, Phys. Rev. B **77,** 165408 (2008).

[21] S. K. H. Lam and D. L. Tilbrook, Appl. Phys. Lett. **82,** 1078 (2003).

[22] R. F. Broom and E. H. Rhoderick, Br. J. Appl. Phys. **11,** 292 (1960).

[23] We get the depairing current [9], $I_d = 2A(2/3)^{3/2}[Hc(0)/\lambda]$ as 1.8 mA at 0 K by using the penetration depth (λ) 200 nm, thermodynamic critical field [$\mu_0 H_c(0)$] 0.2 T, and the cross-section area (A) for each WL as 31×70 nm^2.

[24] T. A. Fulton and L. N. Dunkelberger, Phys. Rev. B **9,** 4760 (1974).

[25] P. Dubos, H. Courtois, B. Pannetier, F. K. Wilhelm, A. D. Zaikin, and G. Schön, Phys. Rev. B **63,** 064502 (2001).